International Journal of Nanomedicine

Dovepress

open access to scientific and medical research

Open Access Full Text Article

ORIGINAL RESEARCH

Novel Timosaponin AIII-Based Multifunctional Liposomal Delivery System for Synergistic Therapy Against Hepatocellular Carcinoma Cancer

Lijuan Zhang[1,*]
Shengan Zhang[2,*]
Min Jiang[1]
Lu Lu[3]
Yue Ding[3]
Ninghui Ma[1]
Yuan Zhao[4]
Sihan Xuchen[1]
Nailian Zhang[1]

[1]School of Pharmacy, Shanghai University of Traditional Chinese Medicine, Shanghai, People's Republic of China; [2]School of Basic Medicine, Shanghai University of Traditional Chinese Medicine, Shanghai, People's Republic of China; [3]Experiment Center for Teaching and Learning, Shanghai University of Traditional Chinese Medicine, Shanghai, People's Republic of China; [4]Center of Science and Technology, Shanghai University of Traditional Chinese Medicine, Shanghai, People's Republic of China

*These authors contributed equally to this work

Introduction: As high cholesterol level has been reported to be associated with cancer cell growth and cholesterol is vulnerable to oxidation, the conventional liposomes including cholesterol in the formulation seem to be challenged. Timosaponin AIII (TAIII), as a steroid saponin from *Anemarrhena asphodeloides* Bunge, possesses a similar structure with cholesterol and exhibits a wide range of antitumor activities, making it possible to develop a TAIII-based liposome where TAIII could potentially stabilize the phospholipid bilayer as a substitution of cholesterol and work as a chemotherapeutic drug as well. Meanwhile, TAIII could enhance the uptake of doxorubicin hydrochloride (DOX) in human hepatocellular carcinoma (HCC) cells and exhibit synergistic effect. Thus, we designed a novel thermally sensitive multifunctional liposomal system composed of TAIII and lipids to deliver DOX for enhanced HCC treatment.

Methods: The synergistic effects of DOX and TAIII were explored on HCC cells and the tumor inhibition rate of TAIII-based liposomes carrying DOX was evaluated on both subcutaneous and orthotopic transplantation tumor models. TAIII-based multifunctional liposomes were characterized.

Results: Synergistic HCC cytotoxicity was achieved at molar ratios of 1:1, 1:2 and 1:4 of DOX/TAIII. TAIII-based liposomes carrying a low DOX dose of 2 mg/kg exhibited significantly enhanced antitumor activity than 5 mg/kg of DOX without detected cardiotoxicity on both subcutaneous and orthotopic transplantation tumor models. TAIII-based liposomes were characterized with smaller size than cholesterol liposomes but exhibited favorable stability. Mild hyperthermia generated by laser irradiation accelerated the release of DOX and TAIII from liposomes at tumor site, and cell permeability of TAIII enhanced uptake of DOX in HCC cells.

Conclusion: The innovative application of TAIII working as bilayer stabilizer and chemotherapeutic drug affords a stable multifunctional liposomal delivery system for synergistic therapy against HCC, which may be referred for the development of other types of saponins with similar property.

Keywords: doxorubicin, timosaponin AIII, liposomes, hepatocellular carcinoma, cholesterol

Correspondence: Lu Lu; Yue Ding
Experiment Center for Teaching and Learning, Shanghai University of Traditional Chinese Medicine, Shanghai, People's Republic of China
Email yjll66@outlook.com; dingyue-2001@hotmail.com

Introduction

Liposomes are the first nano drug delivery systems to be successfully transferred into real-time clinical applications and a number of liposome-based products are available for human use to treat cancers (eg, Doxil®, DaunoXome®, Myocet®).[1] The mentioned liposomal drugs approved for clinical application all contain

Received: 31 March 2021
Accepted: 24 June 2021
Published: 16 August 2021

cholesterol in the formulations because cholesterol was found to reduce the fluidity, stabilize the bilayer and decrease the leakage of contents.[2–4] The presence of rigid steroid polycycle skeleton in cholesterol structure provides optimum strength to the bilayer and up to 50% of cholesterol (in molar) with respect to total lipid excipients is often included in the preparation of liposomes. However, cholesterol is vulnerable to oxidation, leading to a variety of cholesterol oxidation products (COPs), which can be generated during liposome manufacturing and/or storage.[5] COPs, as the major impurities present in liposomal drug products will have a different orientation between the phospholipid molecules due to the more polar property than cholesterol and may influence the quality and the safety of liposomes. On the other hand, increasing studies have reported that high cholesterol level is involved in the development of cancers such as liver, breast, prostate and colorectal cancer.[6–9] Clinical and experimental evidence supports that changes in cholesterol metabolism are associated with a higher cancer incidence, and cholesterol-lowering drugs (eg, statins) exhibit beneficial effects by reducing the risk and mortality of cancer.[10–12] Thus, the presence of cholesterol in conventional liposome-based products may be not friendly to the anti-tumor effect, even counterproductive, once the liposomes degrade in tumor cells. In addition, cancers are complex diseases involving multiple pathways. Chemotherapy with a single chemotherapeutic agent often insufficiently suppresses tumors and even causes drug resistance and side effect. For example, doxorubicin exhibits serious adverse effects, such as lethal cardiotoxicity and dose-limiting myelosuppression, and sorafenib is associated with serious adverse side effects and drug resistance.[13,14] As combination chemotherapy with two or more agents targeting different or similar pathways in the cancer process has been typically used to increase the chances of eliminating cancers,[15] it is expected to design a novel and stable liposomal delivery system with high loading capacity to resolve these challenges.

Small molecule natural products have become one of the most important resources of novel leading compounds especially for the cancers.[16–19] The steroidal saponin compounds, widely distributed in traditional Chinese medicine (TCM) have attracted much attention especially for the prevention and treatment of tumors with low toxicity and high efficiency.[20,21] Timsaponin AIII (TAIII), as a steroidal saponin from *Anemarrhena asphodeloides* Bunge, possess a wide range of antitumor activities, such as inhibiting proliferation, inducing apoptosis and autophagy, and regulating the tumor microenvironment, through multiple related signaling pathways.[22–25] In our lab, in vitro studies have shown that TAIII resulted in apoptosis in HepG2 and HCC-LM3 cells and synergistically inhibited human hepatocellular carcinoma (HCC) cells when combined with Doxorubicin hydrochloride (DOX). But because of the hydrophobicity of TAIII,[26,27] it is challenging to deliver TAIII and DOX simultaneously to the tumor site in vivo and achieve improved tumor inhibiting effects. The key to successful combination therapy is designing a simple codelivery system, which is easy to prepare and can load hydrophobic TAIII and hydrophilic DOX simultaneously to minimize dose amounts and side effects.

Few studies indicate that some saponins are able to insert into bilayers composed of phospholipids in the absence of cholesterol.[28] For example, digitonin can be bound by equilibrium binding (no full insertion) to membranes composed solely of egg yolk phosphatidylcholine and α-hederin is able to bind to the membrane composed of 1,2-dimyristoyl-sn-glycero-3-phosphocholine (DMPC). Furthermore, Hong reported ginsenoside Rh2 could improve physical and chemical properties of phospholipid bilayer.[29] But the aforementioned compounds are triterpenoid pentacyclic saponin. The interaction of steroid pentacyclic saponin with lipid membranes remains to be investigated. Like other steroidal saponins, TAIII contains a core structure of hydrophobic steroid backbone (as shown in Figure 1) that is similar to the structure of cholesterol. The structure shows huge adjuvant potential as the substitution of cholesterol and may be used in the formulation of liposomes. In our previous work,[30] TAIII was entrapped in liposomes composed of 1,2-Dioctadecanoyl-sn-glycero-3-phophocholine (DSPC) and 1, 2-distearoyl-sn-glycero-3- phosphoethanolamine-N-[methoxy (polyethylene glycol)-2000] (DSPE-PEG2000) and the liposome system has been stable in the absence of cholesterol, indicating the possibility of TAIII as adjuvant.

Therefore, taking advantage of the adjuvant potential and anti-tumor activity of TAIII, a novel thermally sensitive liposomal delivery system composed of TAIII, 1, 2-distearoyl-rac-glycero-3-phosphocholine (DPPC) and DSPE-PEG2000 has been developed to encapsulate doxorubicin hydrochloride. As presented in Figure 1, cholesterol was substituted by TAIII in the liposome and TAIII works as membrane stabilizer and chemotherapy drug.

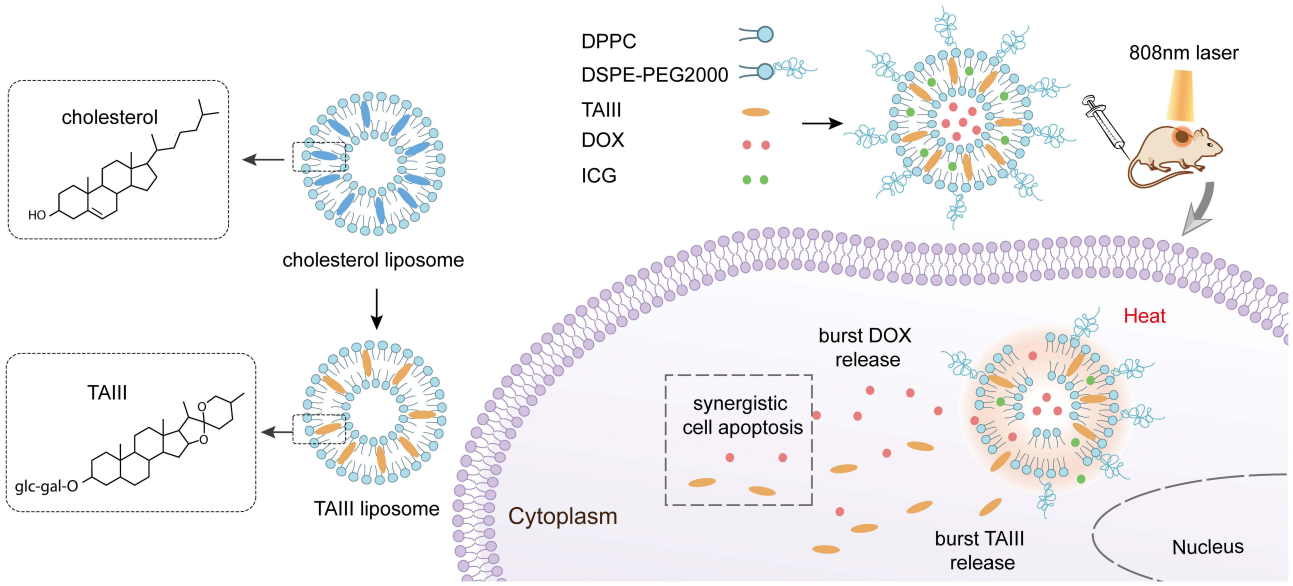

Figure 1 Schematic design of novel TAIII-based multifunctional liposomal delivery system. Novel TAIII-based multifunctional liposomal delivery system was designed in which the membrane stabilizer cholesterol was substituted by TAIII and thermo-sensitive release of DOX and TAIII was induced by NIR irradiation for synergistic therapy against HCC.

Moreover, TAIII is expected to exert anti-tumor activity in HCC cells and induce apoptosis synergistically with DOX.

To enhance the local release of drugs at tumor sites, hyperthermia generated by light or heat cooperating with thermally sensitive liposomes appears the most advanced application and has been used in increasing amounts of research.[31–33] However, hyperthermia generated by external heat or photothermal therapy (PTT) at disease sites often leads to burning of normal tissues under efficient therapies, as observed in the photos of tumor-bearing mice in some studies.[34,35] To overcome this drawback, administering mild hyperthermia (40–45°C) which would not only avoid normal tissue damage but also can promote thermally sensitive carriers for releasing drugs is anticipated. Mild hyperthermia can be realized by adjusting the photosensitizer dosage, irradiation time and intensity in our previous work. Among commonly used photosensitizers, indocyanine green (ICG), a safe and well-tolerated near-infrared (NIR) dye approved by the United States Food and Drug Administration,[36] was chosen in this study to help thermally sensitive liposomes rapidly release encapsulated TAIII and DOX under mild thermal warming (40–45°C) after appropriate irradiation, as presented in Figure 1. Thus, a TAIII-based thermally sensitive liposomes to deliver DOX was designed to achieve a synergistic therapeutic effect and burst drug release at the tumor site was realized by the photothermal conversion effect of ICG, contributing to improved anti-tumor efficacy.

Methods

Materials

DPPC and DSPE-PEG2000 were purchased from Shanghai Advanced Vehicle Technology Pharmaceutical Co., Ltd (Shanghai, China). DOX was purchased from Shanghai Yuanye Biotechnology co., Ltd (Shanghai, China). TAIII was prepared according to the previous report.[37] The structure was confirmed to be TAIII. Near infrared dye Indocyanine green (ICG) were purchased from Sigma-Aldrich (St Louis, USA). Cell-culture minimum essential media (MEM), Dulbecco's modified Eagle's medium (high glucose, DMEM) and fetal bovine serum (FBS) were purchased from Gibco Thermo Fisher Scientific (USA).

Cells Culture

HepG2 cell line was kindly provided by Stem Cell Bank, Chinese Academy of Sciences (Shanghai, China). HCC-LM3 hepatic cancer cell line stably expressing firefly luciferase gene was purchased from Nanjing cobioer Biotech Co., Ltd. HepG2 cells were cultured with MEM and HCC-LM3 cells were cultured with DMEM containing 10% FBS, 100U/mL penicillin, and 100μg/mL streptomycin in 5% CO_2 and 95% relative humidity at 37°C.

Animals

BALB (Bagg Albino)/c nude mice weighing 20–25 g (5–6 weeks old) were supplied by Shanghai Sippr-BK laboratory animal Co., Ltd. (Shanghai, China). All care and handling of the animals was performed in accordance with the requirements of the animal care of Shanghai University of Traditional Chinese Medicine. All experimental protocols have been reviewed and approved by the Institutional Animal Experimental Ethics Committee of Shanghai University of Traditional Chinese Medicine (Approval file No. SZY20170006).

Preparation of TAIII-Based Thermally Sensitive Liposomes

TAIII-based thermally sensitive liposomes (TAIII-LPs) were prepared through thin-film evaporation and an ultrasonic technique. Briefly, DPPC and DSPE-PEG2000 were dissolved in chloroform at a molar ratio of 5:1, and TAIII was dissolved in methanol. The solutions were mixed and evaporated using a rotary evaporator at 60°C for approximately 20 min to form a solid film. The resulting thin film was hydrated in phosphate-buffered saline (PBS) at 60°C to create a suspension followed by incubation for 1h. Next, the suspension was sonicated with an ultrasound probe (2 s sonication followed by 3 s rest) in ice bath for 30 min.

To load DOX, the DOX solution in PBS (1 mg/mL) was added to the mentioned suspension at a molar ratio of 1:4 (DOX: TAIII) followed by incubation for 1h and sonication for 30 min to form DOX loaded liposomes (TAIII-DOX-LPs). To additionally encapsulate a photosensitizer, ICG was incorporated in the lipid layer of liposome by being dissolved in the methanol and mixed with the lipid and TAIII solutions followed by rotary evaporation, hydration with DOX solution, and an ultrasonic process. The molar ratio of ICG in MLPs was 1.2% to prepare multifunctional liposomes (MLPs).

Liposome Characterization

The particle size and zeta potential of TAIII-based liposomes were measured using a Malvern Zetasizer ZEN3600 Nano ZS (Malvern Instruments, Malvern, UK) at 25°C. The surface morphology of TAIII-based liposomes was observed using a JEM-2100 transmission electron microscope (JEOL Ltd., Japan) with a negative stain method. To determine the entrapment efficiency, free DOX, TAIII and ICG in the supernatant was removed using a Sephadex G-50 gel minicolumn. Briefly, 0.2 mL liposomes were placed on a Sephadex G-50 gel minicolumn with 0.6 mL distilled water as the eluent. The eluent was collected after being centrifuged at 4000 rpm for 10 min and considered as encapsulated drug, which was determined after de-emulsification with methanol. DOX was determined through high-performance liquid chromatography (HPLC) and TAIII was measured through HPLC equipped with an evaporative light-scattering detector (HPLC–ELSD) as described in the Supplementary material. ICG was determined through a fluorescence spectrophotometer. Drug loading efficiency (DL) was calculated: DL (%) = molar weight of encapsulated drug/molar weight of liposome × 100%. Entrapment efficiency (EE) was calculated: EE (%) = molar weight of encapsulated drug/molar weight of feeding drug × 100%.

Stability of TAIII-Based Liposomes

To evaluate the stability of TAIII-based liposomes, changes in size were observed at 4°C for 1 week. To further determine the stability in blood, TAIII-based liposomes were incubated with 10% fetal bovine serum, and changes in the average size and polydispersity index (PDI) were measured for 48 h. DOX leakage from the liposomes was also monitored for 48 h at 37°C. Each sample had three replications.

Thermo-Sensitive Release of DOX and TAIII from MLPs

The release of DOX and TAIII from MLPs was investigated through dialysis. Briefly, 1 mL of MLPs was loaded into a dialysis bag (molecular-weight cutoff of 6000–8000 Da; Spectra/Por, USA). The dialysis bags were immersed into PBS and agitated using a magnetic stirrer at 37°C and 42°C for 48 h. Because of the poor solubility of TAIII, the release medium for TAIII used PBS containing 0.5% Tween 80 (v:v). Given that the concentration of TAIII in the release medium was lower than the detectable limit, liposomes in the dialysis bag were measured using HPLC–ELSD at a predetermined time.

Temperature Changes Induced by NIR Irradiation

TAIII-DOX-LPs and MLPs were firstly irradiated by NIR at 808 nm (2W/cm^2) to confirm the photothermal property of ICG. Temperature increments from NIR irradiation in

each sample were measured using a probe thermometer. Based on the temperature increments result, the release rate of DOX and TAIII from MLPs was measured after MLPs were exposed to NIR light at 0.8 W/cm^2 for 5 min.

In vitro Cellular Uptake

The cellular uptake of the MLPs was evaluated in HepG2 cells using a confocal laser scanning microscope (CLSM). Cells were seeded onto glass-bottomed culture dishes at a cell density of 2×10^4 cells/well and incubated for 24 h at 37°C. Free DOX, TAIII, ICG, the mixture of the three drugs and MLPs (final DOX concentration = 0.5 μM; TAIII concentration = 2 μM; ICG concentration = 0.5 μM) were then added to each dish and incubated for 6 h and 24 h. After the culture medium was removed, the cells on microscope plates were washed three times with PBS and then fixed with 4% paraformaldehyde solution for 20 min. The cell nuclei were stained with 4′, 6-diamidino-2-phenylindole (DAPI, blue) for 3 min. The cells were then rinsed three times with PBS. The fluorescence images were obtained using CLSM (Leica TCS SP8).

In vitro Cytotoxicity

Synergistic Effect of DOX and TAIII

The combination index (CI) value was applied to evaluate the synergistic effect of DOX and TAIII and was calculated using the following equation: $CI = [(D)_1/(Dx)_1] + [(D)_2/(Dx)_2]$, where D_1 and D_2 represent the doses of Drugs 1 and 2 used in combination to induce a defined effect (eg, 90% cell death). $(Dx)_1$ and $(Dx)_2$ represent the doses of Drugs 1 and 2 used alone, which induce the same effect as does multiple drugs. The CI equation is based on the multiple drug effect equation from the Chou-Talalay method,[38–40] which offers a quantitative definition of additive effect (CI = 1), synergism (CI < 1), and antagonism (CI > 1) in drug combinations.

For cell viability studies, HepG2 and HCC-LM3 cells were, respectively, seeded in 96-well plates at a density of 9×10^3 cells/well and incubated for 24 h. The medium was replaced by different concentrations of DOX and TAIII and a range of fixed molar ratios of the two drugs for 48 h. Then, cells were treated using the cell counting kit-8 assay (CCK-8, Beyotime Biotechnology, China) at 37°C for 1 h. Absorbance was determined at 450 nm by using a microplate reader (Shanghai Bio Gene Biotech Co., Ltd, Shanghai, China), and cell viability was calculated by cell viability (%) = $(A_{treated} - A_{blank})/(A_{control} - A_{blank}) \times 100\%$, where A_{blank}, $A_{treated}$, and $A_{control}$ represent the absorbance for the well with no cells, cells treated with different drug solutions and controlled cells, respectively. The half-maximal inhibitory concentration (IC_{50}) values were calculated and CI values were analyzed using CalcuSyn[40] (v2, Cambridge, UK).

In vitro Cytotoxicity of TAIII-Based Liposomes

The toxicity of DOX, TAIII, ICG, TAIII-DOX-LPs and MLPs against HepG2 and HCC-LM3 cells was investigated using the CCK-8-based assay. HepG2 and HCC-LM3 cells were, respectively, seeded in 96-well plates at a density of 9×10^3 cells/well and incubated for 24 h. The medium was replaced by different concentrations of DOX, TAIII, DOX/TAIII (at a molar ratio of 1:4), DOX/TAIII/ICG (at a molar ratio of 1:4:1), TAIII-DOX-LPs and MLPs solution for 48 h. Cells were then treated with the CCK-8-based assay at 37°C for 1 h. Absorbance was determined at 450 nm by using a microplate reader, and cell viability was calculated through the aforementioned method. Half-maximal inhibitory concentration (IC_{50}) values were calculated.

Effect of NIR Irradiation on MLPs Cytotoxicity

The effects of NIR irradiation on the cytotoxicity of TAIII-DOX-LPs and MLPs against HepG2 and HCC-LM3 cells were investigated using the CCK-8-based assay. HepG2 and HCC-LM3 cells were prepared and then treated with TAIII-DOX-LPs and MLPs. They then remained in the incubator for 2 h, followed by irradiation with an NIR 808-nm laser at 2 W/cm^2 for 2 min. The CCK-8-based assay was then used to evaluate cell viability by using the aforementioned method.

In vivo Near-Infrared Imaging and Biodistribution

The tumor-bearing BALB/c nude mice model was prepared through the subcutaneous injection of 0.1 mL HepG2 cell suspension (5×10^7 cells/mL) into the right sides of their backs. For the in vivo distribution, tumor-bearing mice were randomly assigned to two groups with three mice per group: ICG and MLPs. ICG and MLPs were administered in amounts of 200 μL through the tail vein. In vivo near-infrared imaging was taken using an IVIS Lumina XR Imaging System (Caliper Life Sciences, PerkinElmer, Inc.). To further monitor tumor accumulation, mice were anesthetized with 1.5% isoflurane at 1:2 O_2/N_2; the IVIS imaging system (excitation of 745 nm) was used to view the tumor accumulation profile. Mice

were sacrificed after 24 h and the tumor, heart, liver, kidney, lung, and spleen were excised. These organs were also imaged at the aforementioned excitation wavelength.

In vivo Photothermal Imaging

Tumor-bearing mice (3 mice per group) were prepared as aforementioned and treated with PBS, ICG (1mg/kg), TAIII-DOX-LPs (DOX 2 mg/kg, TAIII 10 mg/kg), and MLPs (DOX 2 mg/kg, TAIII 10 mg/kg, ICG 1mg/kg). Thermal images of tumor-bearing mice were recorded by an infrared thermal camera (FLIR Systems, Wilsonville, OR, USA) before and after tumors were exposed to an 808-nm laser (1.5 W/cm^2) for a 10-min postinjection. Mice receiving PBS were used as the control.

In vivo Antitumor Activity on the Subcutaneous Transplantation Tumor Model

The tumor-bearing BALB/c nude mice model was prepared as aforementioned. When the tumor volume reached approximately 100 mm^3, tumor-bearing mice were randomly assigned to seven groups (n = 6 per group): control group, control group combined with laser irradiation, DOX-treated group (2 and 5 mg/kg, respectively), TAIII-LPs-treated group (10 mg/kg), MLPs-treated group (DOX dose = 2 mg/kg, TAIII dose = 10 mg/kg, ICG = 1mg/kg), and the group treated with MLPs combined with laser irradiation. The control group and control group combined with laser irradiation were intravenously injected with PBS, and the other groups were intravenously injected with a drug solution or liposomes 3 times per week. For laser irradiation, tumors were exposed to an 808-nm laser for a 10-min postinjection lasting for 5 min at a power density of 1.5 W/cm^2. The weight of mice and tumor volumes were measured 3 times per week throughout the study. Tumor volumes (mm^3) were calculated as length × (width)^2/2. After 3 weeks, mice were sacrificed and tumors were collected and weighed. The tumor inhibitory rate was calculated as $(W_C - W_A)/W_C \times 100\%$, where W_C and W_A are the mean weight of tumors in the control and drug-treated groups, respectively. In addition, the tumor, heart, liver, kidney, lung, and spleen were excised from the sacrificed mice of each group and fixed with 4% paraformaldehyde solution, followed by paraffin embedding. The sliced organ tissues were then stained with hematoxylin and eosin (H&E) to assess histological alterations through a digital microscope. Meanwhile, tumor tissue apoptosis was observed using a digital microscope through terminal deoxynucleotidyl transferase dUTP nick end labeling (TUNEL) staining.

In vivo Antitumor Activity on the Orthotopic Transplantation Tumor Model

The orthotopic transplantation tumor model was successfully established in our labs,[41] which was similar to the reported method[42] and prepared as described in the Supplementary material. Successful orthotopic hepatoma–bearing mice were randomly assigned into five groups (n = 5 per group). One group was intravenously injected PBS as the control, and the other four groups were intravenously injected DOX solution (2 mg/kg), DOX solution (5 mg/kg), TAIII-LPs (10 mg/kg), and TAIII-DOX-LPs (DOX dose = 2 mg/kg, TAIII dose = 10 mg/kg). The weight of mice was measured 3 times per week throughout the study. Tumor growth was assessed by measuring luminescence from HCC-LM3 cells using the IVIS Lumina XR Imaging System. After 4 weeks, mice were sacrificed and tumors were collected and weighed. The tumor inhibitory rate was calculated as $(V_C - V_A)/V_C \times 100\%$, where V_C and V_A are the mean volume of tumors in the control group and each drug-treated group, respectively. TUNEL staining of tumors and H&E staining of other organs were performed.

Statistical Analysis

All data are shown as mean ± standard deviation. One-way analysis of variance (ANOVA) was performed using SPSS software to determine the significance of differences among groups. Statistical significance was set at $P < 0.05$.

Results and Discussion

Characterization of TAIII Liposomes

The optimal formulation of TAIII liposomes was assessed from the molar ratio between lipids and drugs. As presented in Figures 2A and B, when the molar ratio of DPPC, DSPE-PEG2000, and TAIII was set at 5:1:4, 5:1:2, 5:1:1, and 10:2:1, DOX could be efficiently encapsulated in an internal aqueous environment, with EE ranging from 30.0% to 88.7% and DL ranging from 0.9% to 2.2%. Although TAIII has affinity to the phospholipid bilayer and works as a substitute for cholesterol, it also works as a chemotherapeutic drug. Therefore, the EE and DL of TAIII was determined. EE of TAIII ranges from 20.6% to

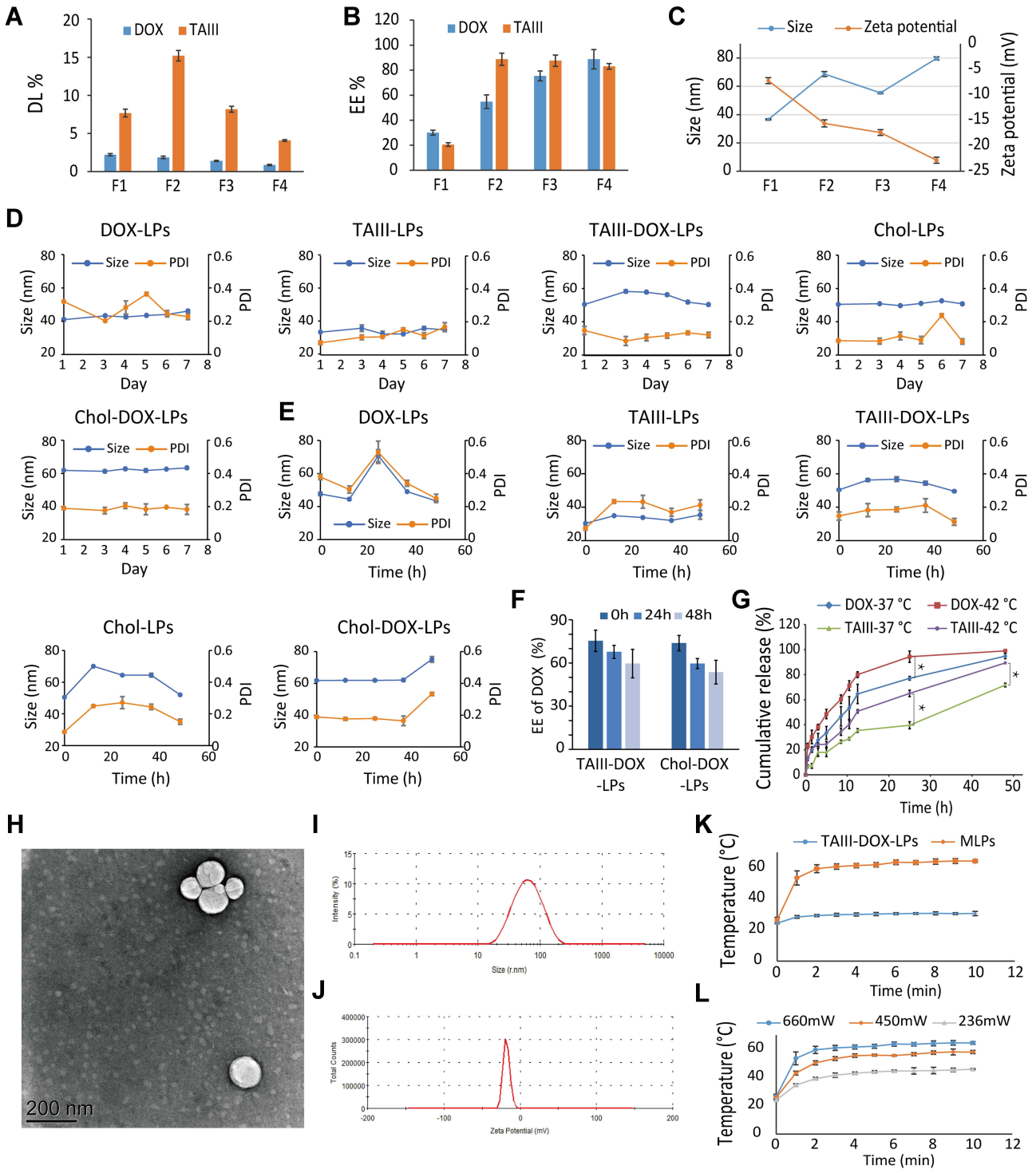

Figure 2 Characteristics of TAIII-based liposomes. (**A**) DL of TAIII-DOX-LPs at various molar ratios of lipid and drugs (n = 3). (**B**) EE of TAIII-DOX-LPs at various molar ratios of lipid and drugs (n = 3). (**C**) TAIII-DOX-LPs size and zeta potential at different molar ratios of lipid and drugs (n = 3). F1, F2, F3 and F4 represent 5:1:4, 5:1:2, 5:1:1 and 10:2:1 of DPPC, DSPE-PEG2000 and TAIII, respectively (n = 3). (**D**) Stability of cholesterol and TAIII liposomal formulations kept in 4°C conditions. (**E**) Stability of cholesterol and TAIII liposomal formulations kept in 10%FBS. (**F**) DOX leakage of the two liposomal formulations stored at 4°C conditions. (**G**) Cumulative release profile of DOX and TAIII from MLPs in PBS at 37°C and 42°C. (**H**) TEM image of MLPs. (**I**) Size distribution by intensity of MLPs. (**J**) Zeta potential distribution of MLPs. (**K**) Temperature change of TAIII-DOX-LPs and MLPs induced by NIR at 660mW. (**L**) Temperature increment of MLPs induced by NIR at 660, 450 and 236mW, respectively. All values are represented as mean ± SD (n = 3).* $P < 0.05$.

https://doi.org/10.2147/IJN.S313759 DovePress

88.7% and DL of TAIII ranges from 4.1% to 15.2%. High feed amounts of lipids caused the increased EE of DOX and TAIII. However, the highest DL (2.2% ± 0.2%) of DOX was obtained at F1 (5:1:4), and the highest DL (15.2% ± 0.7%) of TAIII was obtained at F2 (10:2:1). In addition, the size and zeta potential of TAIII-DOX-LPs ranged from 36.6 to 79.7 nm and −7.2 to −22.8 mV, respectively, depending on different molar ratios (Figure 2C). To achieve a high DL and EE with both DOX and TAIII, the molar ratio of DPPC, DSPE-PEG2000 and TAIII was fixed at 5:1:1, with a high EE (78.6% ± 5.9%) and an appropriate DL (1.9% ± 0.3%) for DOX.

The conventional cholesterol liposomes (Chol-LPs) were easily prepared following the procedures for the manufacture of TAIII liposomes. The particle size, PDI and zeta potential of different formulations are presented in Table 1. TAIII liposomes were smaller than cholesterol liposomes and the zeta potential of TAIII liposomes was much lower than cholesterol liposomes. EE of DOX was similar in TAIII liposomes and cholesterol liposomes. The stability of the liposomes was determined by evaluating the changes in their size over time when the liposomes were stored at 4°C for 7 days and in 10% FBS for 48 h. TAIII liposomes and cholesterol liposomes were stable during the test period with negligible changes in size and PDI (Figure 2D and E). However, size and PDI of DOX-LPs in the absence of TAIII or cholesterol fluctuated over time when DOX-LPs were stored in 10% FBS for 48h, and PDI of DOX-LPs stored at 4°C changed clearly, indicating the necessary of membrane stabilizer. Moreover, DOX leakage test (Figure 2F) indicated that TAIII-DOX-LPs exhibited a less DOX leakage compared with that in Chol-DOX- LPs at 24h and 48h, indicating the potential of TAIII as bilayer stabilizer.

Based on the optimal liposomal formulation, MLPs were prepared containing 1.2% (in molar) ICG. In MLPs, the DL of DOX and TAIII was 1.4% ± 0.1% and 8.2% ± 0.4%, respectively, and the EE of DOX and TAIII was 75.4% ± 7.4% and 87.5% ± 4.5%, respectively. Meanwhile, the DL and EE of ICG was 1.9% ± 0.2% and 74.9% ± 6.4%, respectively. Additive encapsulation of ICG produced little effect on the DL and EE of DOX and TAIII, and this indicated the desired multiple drug loading capacity of TAIII-based liposomal formulation. Transmission electron microscopy (TEM) verified that MLPs had a well-defined spherical shape and were homogeneously distributed (Figure 2H). The average diameters of MLPs were 55.4 ± 0.4 nm, with a polydispersity index of 0.23 ± 0.02 (Figure 2I), and a suitable particle size and distribution for targeted drug delivery.[43] The zeta potential of MLPs was determined to be −17.4 ± 0.6 mV (Figure 2J). Small nanoparticles with a size of 10–100 nm have been considered to be beneficial for a rapid cellular internalization and lower clearance by reticuloendothelial system (RES) in comparison to larger particles (>200 nm), and a previous study showed that negatively charged quantum dots were internalized much faster than neutral or positively charged quantum dots.[44] Therefore, the small particle size and weak negative charge of MLPs might permit the favorable in vivo tumor accumulation and transport of nanoparticles through enhanced permeability and retention (EPR) effect.

In vitro Release of DOX and TAIII from MLPs

The effect of temperature on release of DOX and TAIII from the thermosensitive liposomes was evaluated at 37°C and 42°C, respectively. As illustrated in Figure 2G, the extents of DOX and TAIII released from MLPs at 37°C were comparatively less than that at 42°C. After 12 h, only 64.6% of DOX and 35.4% of TAIII were released from MLPs at 37°C whereas 80.0% of DOX and 50.7% of TAIII were released at 42°C. After 24 h, MLPs exhibited an approximately 77.1% and 39.6% cumulative release for DOX and TAIII at 37°C, respectively. The cumulative

Table 1 Basic Characterization of Cholesterol Liposomes and TAIII-Based Liposomes

	Size (nm)	PDI	Zeta Potential (mV)	EE (%)	
				DOX	TAIII
Chol-LPs	55.5±0.1	0.086±0.007	−9.6±0.3	/	/
Chol-DOX- LPs	68.8±0.2	0.189±0.008	−8.6±0.6	73.8±5.3	/
TAIII-LPs	32.0±0.2	0.073±0.011	−16.2±0.5	/	90.4±4.3
TAIII-DOX-LPs	55.4 ± 0.4	0.147 ± 0.024	−17.4 ± 0.6	76.3 ± 3.9	88.9 ± 5.5

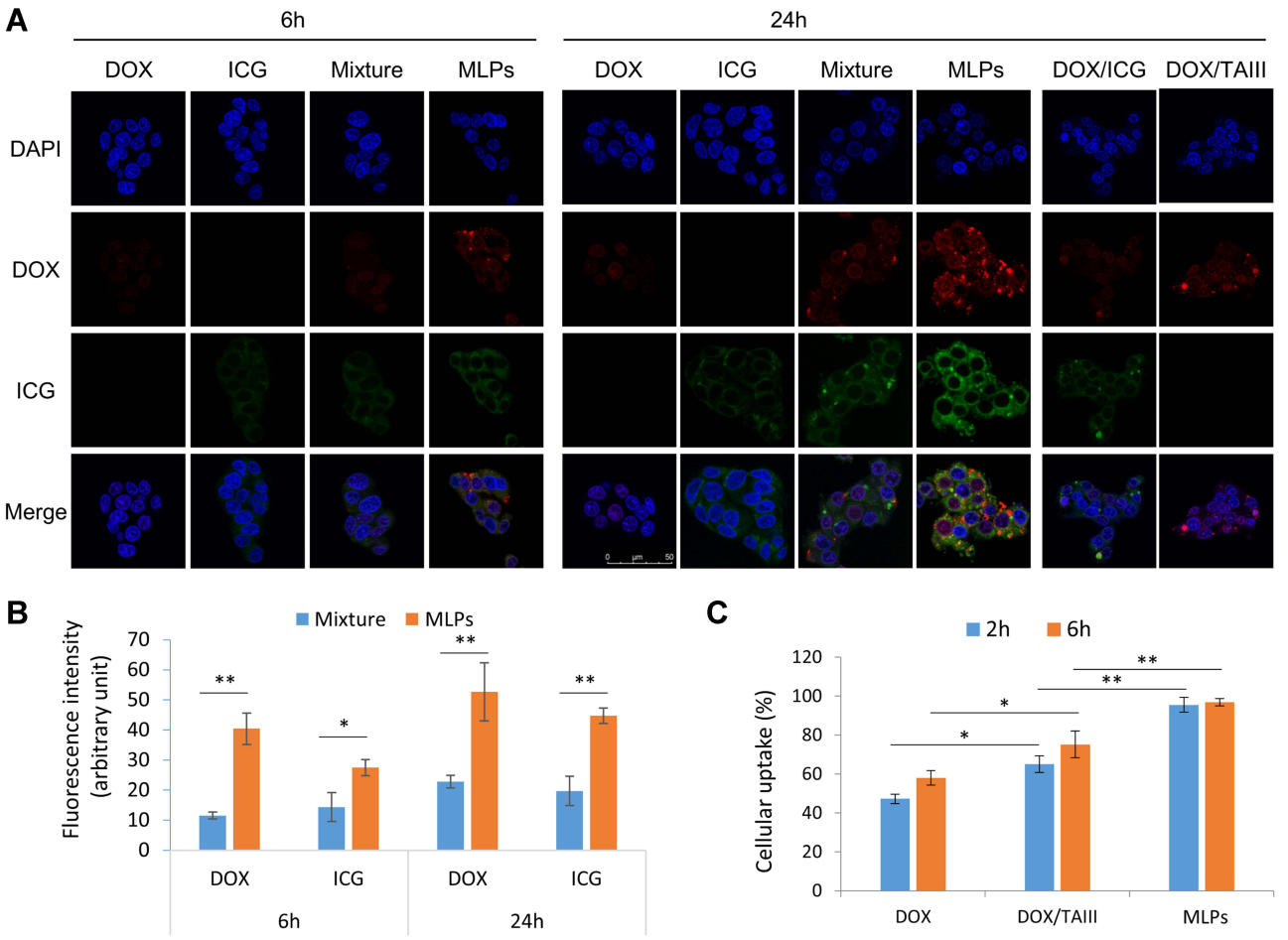

Figure 3 The cellular uptake of free drugs and MLPs in HepG2 cells. (**A**) CLSM images of HepG2 cells after incubation with DOX; ICG; a mixture of DOX, TAIII, and ICG; and MLPs. For each panel, images from the top down present nuclei stained by DAPI (blue), DOX fluorescence in cells (red), ICG fluorescence in cells (green), and overlays of the three images. (**B**) The quantitative fluorescence intensity of DOX and ICG in the mixture and MLPs in HepG2 cells. (**C**) Cellular uptake of DOX detected using a flow cytometry in DOX, mixture of DOX and TAIII, and MLPs groups. The images were obtained at 630× magnification. *$P < 0.05$. **$P < 0.01$.

release at 42°C was 94.3% for DOX and 65.0% for TAIII, which was 1.2 and 1.6-fold greater than that at 37°C, respectively. The results suggested that a temperature of 42°C accelerated the release rate of DOX and TAIII from MLPs.

Temperature Increment Induced by NIR Irradiation

Figure 2K indicates that the temperature of MLPs after exposure to 808-nm NIR laser irradiation for 10min could increase to 60°C. By contrast, the temperature of TAIII-DOX-LPs without ICG remained at approximately 25°C after NIR laser irradiation for 10min, which suggested that heat induced by laser irradiation was ICG-dependent. Figure 2L illustrates that the MLPs temperature increment induced by NIR laser irradiation was related to the radiation intensity. When MLPs were exposed to 808-nm NIR laser irradiation for 2 min at 236, 450, and 660mW, the temperature was 39.2±1.0°C, 45.2±1.4°C and 59.5±2.6°C, respectively. In vitro photothermal imaging photos are displayed in Figure S1 in the Supplementary material. Furthermore, photothermal stability of ICG in MLPs was assessed and results was shown in Figure S2. The photothermal conversion effect of ICG in MLPs was relatively stable in 30 days.

Given that 45.2°C can accelerate the release rate of DOX and TAIII from MLPs while remaining harmless to normal tissues, 450mW (0.8 W/cm^2) was selected as the optimal radiation intensity for drug release study. To evaluate the NIR irradiation triggered release of DOX and TAIII from MLPs, MLPs were exposed to NIR light for 5 min and the release rate of drugs were determined. The release rate of DOX and TAIII was 56.3% and 50.6%, respectively. The released molar ratio of DOX and TAIII was close to 1:4, within the range of synergistic ratios. The

results indicated that NIR laser irradiation could effectively induce burst release of DOX and TAIII due to the efficient photothermal conversion effect of ICG, which is beneficial to enhance the antitumor efficacy.

In vitro Cellular Uptake

The cellular uptake of free drugs and MLPs in HepG2 cells after 6 and 24 h of incubation is illustrated in Figure 3. Fluorescence in all groups greatly increased as incubation time increased to 24 h (Figure 3A and B). HepG2 cells treated with the mixture of DOX and ICG (shown as DOX/ICG in Figure 3A) for 24 h exhibited equal fluorescence with the two drugs used alone, which indicated that no enhanced uptake was mutually induced by DOX and ICG. When DOX was incubated with TAIII (shown as DOX/TAIII in Figure 3A), the red fluorescence of DOX in HepG2 cells was stronger than when used alone (Figure 3A). Moreover, the cellular uptake of DOX detected by the flow cytometer when incubated with TAIII for 6h was 75.2%±6.8%, higher than that of DOX alone (58.1%±3.7%), as presented in Figure 3C. The results indicated that TAIII enhanced DOX uptake, likely because of the membrane-permeabilizing properties of saponins,[21,45,46] which have been reported to interact with cholesterol in lipid membrane, change the organization of membrane phospholipids, thus leading to enhanced drug transmission.[28] This may have contributed to the enhanced anti-tumor effect of DOX and TAIII combination therapy. As expected, cells treated with MLPs presented stronger fluorescence than did DOX, TAIII, and ICG used together (a mixture), and this was further verified through flow cytometry. The cellular uptake of MLPs detected by DOX fluorescence was 96.9% ±1.8%, which was higher than that of the mixture (75.2%±6.8%). The results revealed that MLPs could better enhance cellular uptake than free drugs.

Synergistic Effects of DOX and TAIII

The synergistic effects of DOX and TAIII were evaluated against HepG2 and HCC-LM3 cells, respectively, which have not yet been explored. DOX and TAIII were exposed to cells alone or combined for 48 h, and CI values were calculated based on cell survival inhibition. As illustrated in Figure 4A and C, when the DOX-TAIII ratio was set at 1:1, 1:2, and 1:4, the cell viability of combination medication on HepG2 and HCC-LM3 cells was lower than that of single DOX and TAIII. Meanwhile, CI values calculated by 50%, 75% and 90% cell survival inhibition were all below 1 in HepG2 and HCC-LM3 cells (Figure 4B and D). The results suggested that combined DOX and TAIII at molar ratios of 1:1, 1:2, and 1:4 provided satisfactory synergistic effects against HepG2 and HCC-LM3 cells with a lower concentration of drugs than with DOX and TAIII alone. However, CI values obtained at a molar ratio of 2:1 against the two cell lines were equal to or higher than 1, which denoted additivity or antagonism. This result was reasonable because when the molar ratio of DOX and TAIII was set at 2:1, the concentration of TAIII was much lower than the effective concentration and could not cause synergistic or additive cytotoxic activity. In addition, Figure 4A and C showed that TAIII barely affected the cell inhibition of DOX at the ratio of 2:1 (DOX/TAIII). Among molar ratios with strong synergistic effects, the molar ratio of 1:4 (DOX/TAIII) was selected for further study. First, the effective dosage of DOX typically used in in vivo antitumor research is 2–5 mg/kg, and 2 mg/kg was applied in this study to prevent DOX from causing cardiotoxicity. Second, in our previous study,[30] a 7.5-mg/kg TAIII liposome dose inhibited tumors by 40.9% on HepG2 tumor–bearing mice. When the dose of TAIII liposomes improved to 10 mg/kg, the molar ratio of DOX and TAIII precisely became 1:4.

Synergistic Therapy of DOX and TAIII Caused Apoptosis in HCC Cells

Previous studies suggested that TAIII could induce apoptosis in various different cancers including colon cancer cells, breast carcinoma cells and human hepatocellular carcinoma cells. Therefore, the apoptosis-inducing effect of DOX and TAIII was further confirmed by flow cytometer in this study. The method and data of apoptosis assay and Western blot analysis were presented in the Supplementary material. As shown in Figure S3A and B, the combination of DOX and TAIII caused more apoptosis in both the two cell lines, especially in TAIII-DOX-LPs treated groups. For HepG2 cells, the apoptosis rate of TAIII-DOX-LPs was 77.2%±1.5%, which is 2.0-fold than that of DOX (38.1%±2.4%) and 3.4-fold than TAIII (22.4%±3.8%), respectively. The apoptosis rate of DOX/TAIII against HepG2 cells was 71.1%±0.6%, which is lower than that of TAIII-DOX-LPs (Figure S3C). The percentages of HCC-LM3 cell apoptosis were 59.6% ±0.4%, 55.3%±1.4%, 65.1%±5.0% and 87.0%±2.7% for DOX, TAIII, DOX/TAIII and TAIII-DOX-LPs, respectively (Figure S3D), and the apoptosis rate of TAIII-DOX-LPs was 1.5- and 1.6-fold than that of DOX and

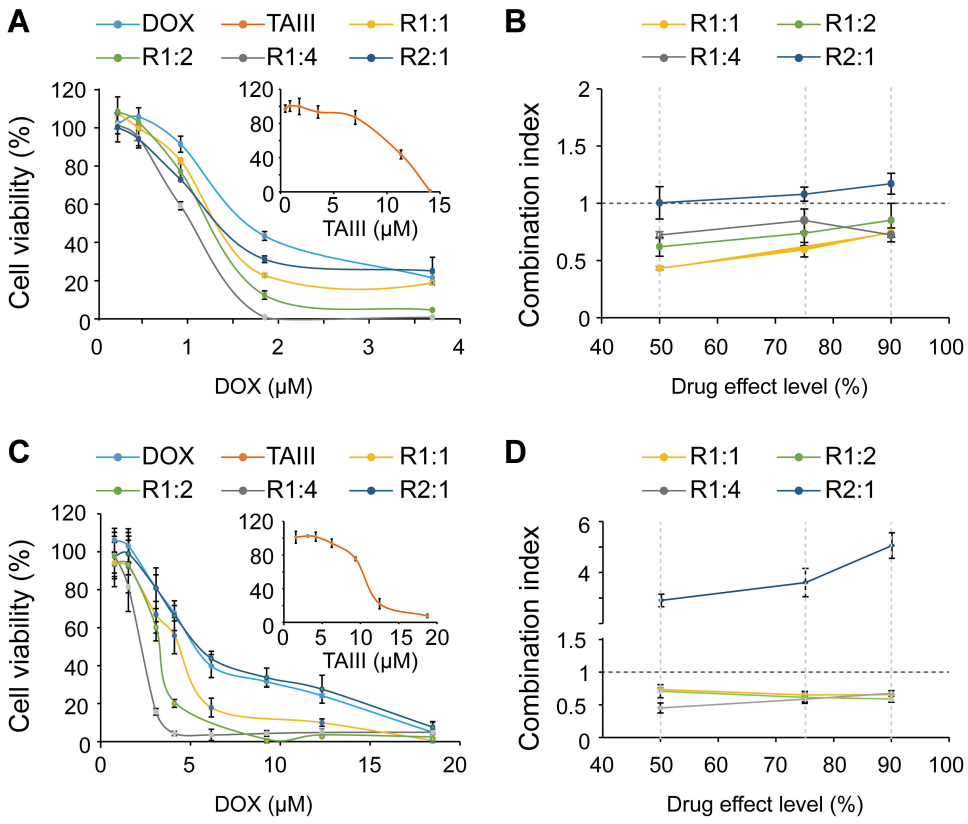

Figure 4 Synergistic effects of DOX and TAIII against HepG2 and HCC-LM3 cells. (**A**) Cell viability of combination of DOX and TAIII at different molar ratios against HepG2 cells. (**B**) CI values calculated by 50%, 75% and 90% cell survival inhibition at different molar ratios of DOX/TAIII against HepG2 cells. (**C**) Cell viability of combination of DOX and TAIII at different molar ratios against HCC-LM3 cells. (**D**) CI values calculated by 50%, 75% and 90% cell survival inhibition at different molar ratios of DOX/TAIII against HCC-LM3 cells.

TAIII. The results suggested that DOX and TAIII co-delivery liposomes significantly enhanced the apoptosis against HepG2 cells and HCC-LM3 cells.

The expression of apoptosis related protein, cleaved forms of caspase-3, caspase-9, caspase-8, Bax and Bcl-2 were evaluated with Western blotting. As shown in Figure S3E and F, the results revealed that remarkable increase of Bax protein, a promoter protein regulating apoptosis, was observed in DOX/TAIII and TAIII-DOX-LPs treated HepG2 cells and TAIII-DOX-LPs treated HCC-LM3 cells. Meanwhile, apoptosis inhibitory protein Bcl-2 in both HepG2 cells and HCC-LM3 cells was decreased by DOX/TAIII and TAIII-DOX-LPs treatment. Furthermore, the activity of caspase family members was studied to evaluate the mechanisms of apoptotic pathways. The active cleaved forms of caspase-9 and caspase-3 protein level were upregulated in DOX/TAIII and TAIII-DOX-LPs treatment group but minute increase was observed in TAIII and DOX treatment groups. In addition, HepG2 cells and HCC-LM3 cells treated with DOX/TAIII and TAIII-DOX-LPs demonstrated a declining trend in the total expression of caspase-8. The results suggested that DOX/TAIII and TAIII-DOX-LPs induced apoptosis in HepG2 cells by both intrinsic and extrinsic pathways and were consistent with previous studies in which TAIII induced mitochondria-mediated apoptosis in many tumor cell lines such as in HCC cells, acute myeloid leukemia cells,[47] human cervical carcinoma HeLa cells,[48] human melanoma A375-S2 cells[23] and human colorectal cancer HCT-15 cells.[49] Although DOX results in intercalation between the base pairs of DNA strands, inhibits DNA and RNA synthesis in rapidly growing cells, and causes oxidative damage to cellular membranes, proteins, and DNA, the additive apoptosis rate was achieved by combining DOX and TAIII. A high level of cleaved caspase-9 and caspase-3 proteins were obtained from DOX/TAIII and TAIII-DOX-LPs treatment against HCC cells than from a single drug, which suggested an intrinsic apoptotic pathway. However, further in vivo or ex vivo studies are required to explore possible mechanisms for synergistic therapeutic effects.

In vitro Cytotoxicity of TAIII-Based Liposomes

The cytotoxicity of DOX, TAIII, DOX/TAIII (at a molar ratio of 1:4), DOX/TAIII/ICG (at a molar ratio of 1:4:1), and TAIII-DOX-LPs and MLPs solution against HepG2 and HCC-LM3 cells was assessed using a CCK-8-based assay. As indicated in Figure S4, blank-LP and free ICG (0–4 μM) were nontoxic to HepG2 and HCC-LM3 cells, which indicated the safe and well-tolerated property of the lipid and ICG. DOX combined with TAIII, TAIII-DOX-LPs and MLPs was significantly more cytotoxic at low concentrations than single DOX and TAIII (Figure 5A and B). After 48-h incubation, TAIII-DOX-LPs and MLPs presented lower IC_{50} values (Tables 2 and 3) for DOX and TAIII than with DOX/TAIII and a single drug, which indicated significantly enhanced antitumor activity against HepG2 and HCC-LM3 cells. The results suggest that DOX and TAIII could be efficiently released from TAIII-DOX-LPs and MLPs in HepG2 and HCC-LM3 cells, and liposome codelivery could effectively enhance cytotoxicity, which was presumably attributable to the enhanced cellular uptake of liposomes through nonspecific endocytosis. The cytotoxicity of DOX/TAIII and DOX/TAIII/ICG treatment had no significant difference, which was the same as that between TAIII-DOX-LPs and MLPs. This suggests that ICG did not affect the synergy between DOX and TAIII, and no additive or antagonistic effects induced by ICG, which can be used as a safe and well-tolerated NIR dye for causing mild hyperthermia in future experiments.

As revealed in previous work (Figure 2K), MLPs temperature increments were induced by NIR laser irradiation with the current ICG; therefore, the heat effect may trigger burst release of DOX and TAIII from MLPs and enhance the proliferation inhibitory rate. HepG2 and HCC-LM3 cells were treated with TAIII-DOX-LPs and MLPs at different concentrations for 2 h and then exposed to NIR laser irradiation. Figure 5C and 5D indicate that NIR laser irradiation did not affect control cells and cells treated with TAIII-DOX-LPs without ICG, whereas enhanced cytotoxicity was induced by laser irradiation in MLPs and ICG-LP-treated cells (Figure 5E and F). The cell viability of MLPs (10.0%±2.6%) was equivalent to that of TAIII-DOX-LPs (11.1% ± 2.2%) treating HepG2 cells without NIR laser irradiation, as presented in Figure 5C and Table 4. But after NIR laser irradiation, the cell viability of the MLPs treated group greatly decreased, and only 1.7%±0.5% of cells survived. However, the cell viability of TAIII-DOX-LPs (11.1% ± 2.2%) and TAIII-DOX-LPs combined with NIR laser irradiation (8.6% ± 1.6%) presented no significant difference. A similar result was produced with HCC-LM3 cells (Figure 5D). The IC_{50} value of ICG-LP against HepG2 and HCC-LM3 cells was above 10 μM. The result also revealed that the ICG included in MLPs of no more than 2 μM do not generate cytotoxic heat but mild hyperthermia to help trigger the release of DOX and TAIII from MLPs. The significant difference between MLPs treatments with/without NIR exposure at all evaluated concentrations against both cell lines suggested that combined chemotherapy and hyperthermia enhanced therapeutic effects.

In vivo NIR Imaging and Biodistribution

In vivo NIR imaging was performed using an IVIS Lumina XR Imaging System to evaluate MLPs biodistribution. As presented in Figure 6A, the ICG fluorescence signal in tumors gradually increased in mice treated with MLPs from 0.2- to 24-h time points, whereas weaker fluorescence signals were observed at the tumor site in the free ICG-treated group. In addition, stronger fluorescence at the tumor site was detected in the MLPs-treated group than in the free ICG-treated group at all observed time points. Furthermore, ex vivo fluorescence (Figure 6B) in tumors in the MLPs-treated group was strong, whereas negligible ICG fluorescence was detected in other major organs in the MLPs-treated group and in all tissues including tumors in the free ICG-treated group. This indicated that TAIII-based liposomes could alter the biodistribution of free ICG and improve drug accumulation at the tumor site, possibly caused by the EPR effect, thus presenting passive targeting activity.

In vivo Photothermal Imaging

An infrared thermal camera was used to record the temperature of tumor sites before and after tumors were exposed to an 808-nm laser (1.5 W/cm^2) with a 10-min postinjection. As displayed in Figure 6C and D, the initial temperature of tumors in all groups was approximately 35°C. After NIR laser irradiation for 10 min, the temperature at tumor sites in PBS- and TAIII-DOX-LPs-treated groups slightly increased to approximately 39°C. The temperature at tumor sites in the ICG-treated group was 42.0 ± 2.2°C and it was 45.1 ± 2.4°C in the MLPs-treated group. The results indicated that ICG could efficiently induce temperature increment at tumor sites through NIR laser irradiation, which would accelerate the release of DOX and TAIII from MLPs in tumors. Accordingly, MLPs combined with NIR laser irradiation may have

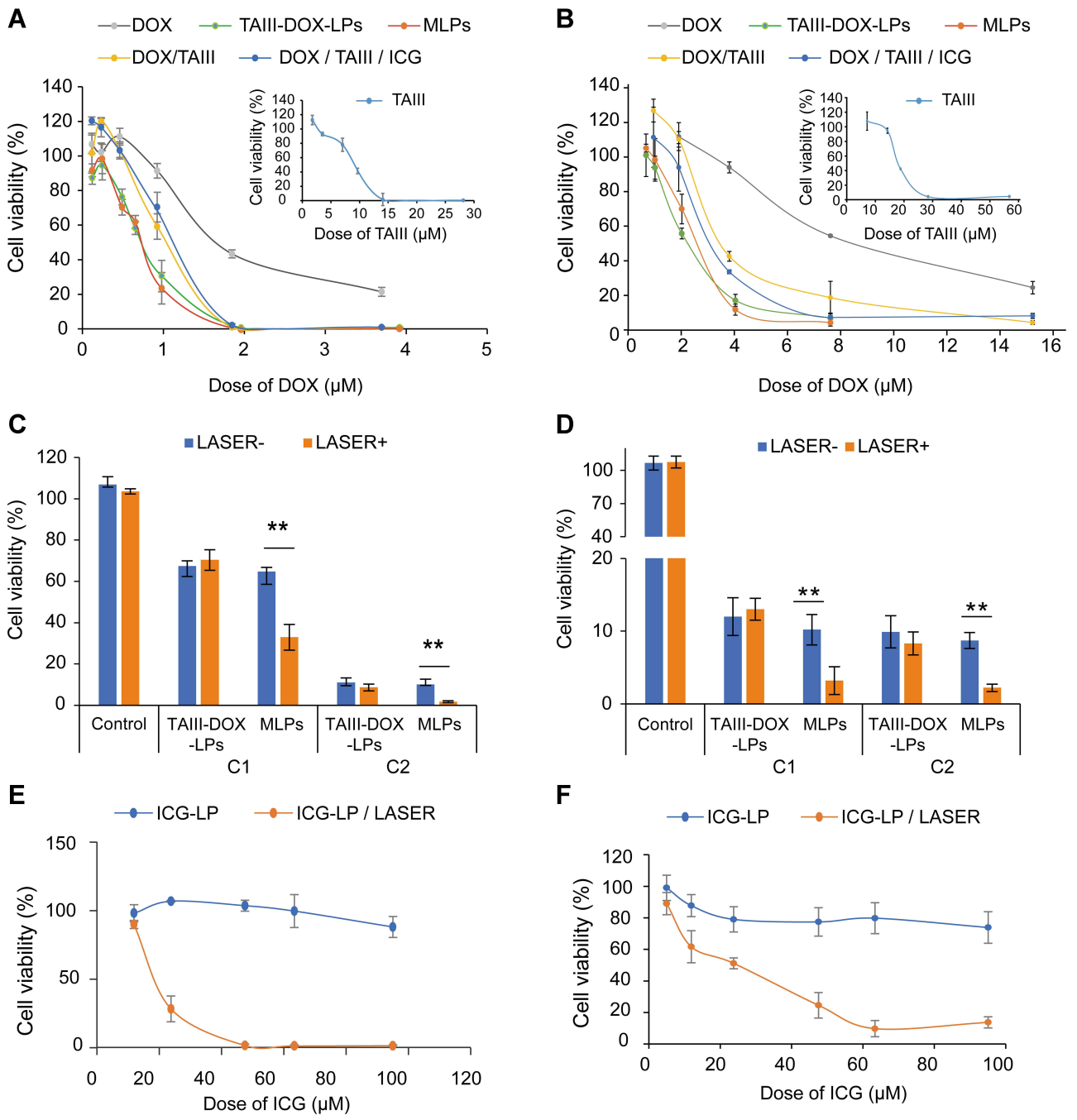

Figure 5 In vitro cytotoxicity of TAIII-based liposomes against HepG2 and HCC-LM3 cells. (**A**) In vitro cytotoxicity of DOX, TAIII, DOX/TAIII, DOX/TAIII/ICG, TAIII-DOX-LPs, and MLPs against HepG2 cells after 48-h incubation. (**B**) In vitro cytotoxicity of DOX, TAIII, DOX/TAIII, DOX/TAIII/ICG, TAIII-DOX-LPs, and MLPs against HCC-LM3 cells after 48-h incubation. (**C**) Effects of laser irradiation on in vitro cytotoxicity of TAIII-DOX-LPs and MLPs against HepG2 cells. (**D**) Effects of laser irradiation on in vitro cytotoxicity of TAIII-DOX-LPs and MLPs against HCC-LM3 cells. (**E**) Effects of laser irradiation on in vitro cytotoxicity of ICG-LP against HepG2 cells. (**F**) Effects of laser irradiation on in vitro cytotoxicity of ICG-LP against HCC-LM3 cells. $^{**}P < 0.01$.

enhanced antitumor efficacy from the pharmacological activity of DOX and TAIII.

In vivo Antitumor Activity

An in vivo antitumor study was evaluated on HepG2 subcutaneous transplantation tumor-bearing mouse models and HCC-LM3 orthotopic transplantation tumor models. Mice treated with PBS were used as the control. As illustrated in Figure 7A, no serious reduction in body weight was observed in all groups except in the 5-mg/kg DOX-treated group, which indicated fine biological compatibility and innocuity of liposomes. Figure 7B presents the changes in

Table 2 In vitro Cytotoxicity of DOX, TAIII, DOX/TAIII, DOX/TAIII/ICG, TAIII-DOX-LPs and MLPs Against HepG2 Cells (n = 3)

IC_{50} (μM)	DOX	TAIII	DOX/TAIII	DOX/TAIII/ICG	TAIII-DOX-LPs	MLPs
DOX	1.42±0.02	–	1.00±0.10*	1.00±0.14*	0.77±0.03**	0.68±0.09**
TAIII	–	7.88 ± 1.08	3.80 ± 0.38##	3.79±0.55##	1.70±0.42##	1.67 ± 0.63##

Notes: *P < 0.05. **P < 0.01, compared to DOX. ##P < 0.01, compared to TAIII.

Table 3 In vitro Cytotoxicity of DOX, TAIII, DOX/TAIII, DOX/TAIII/ICG, TAIII-DOX-LPs and MLPs Against HCC-LM3 Cells (n = 3)

IC_{50} (μM)	DOX	TAIII	DOX/TAIII	DOX/TAIII/ICG	TAIII-DOX-LPs	MLPs
DOX	6.60±1.06	–	3.65±0.55**	2.95±0.67**	2.51±0.36**	2.37±0.29**
TAIII	–	14.20 ± 2.51	12.56 ± 1.06	11.24±2.53#	9.93±1.43#	9.30 ± 1.18#

Notes: **P < 0.01, compared to DOX. #P < 0.05, compared to TAIII.

tumor volume among all groups during the study. NIR laser irradiation had no impact on the tumor growth compared with the control group. As expected, MLPs effectively inhibited tumor growth better than did DOX alone and TAIII-LP on Day 21 (Figure 7B). Images of tumors (Figure 7C) excised from mice on Day 21 presented the enhanced antitumor efficiency of MLPs and a combination therapy of MLPs and NIR laser irradiation. The tumor inhibitory rate of MLPs was calculated to be 61.6% ± 21.4%, which was 1.9- and 1.5-fold higher than that of 2 mg/kg DOX (33.3% ± 17.1%) and TAIII-LP (39.5% ± 26.9%) (Figure 7D), which indicated that TAIII-based liposomes carrying DOX significantly enhanced the antitumor activity of the two drugs with synergistic effects. Notably, MLPs with 2 mg/kg of DOX even exhibited more favorable tumor inhibition than did 5 mg/kg of DOX (53.7% ± 25.4%) without causing loss of body weight and cardiotoxicity (Figures 7A and F). Furthermore, when tumors were exposed to laser irradiation after MLPs injection, tumors grew slowly throughout the experimental period and tumors even disappeared in two mice (Figure 7C). MLPs combined with laser irradiation presented stronger therapeutic efficacy with a tumor inhibitory rate of 85.8% ± 14.5%, which was 1.4-fold that of MLPs alone. The result suggested that 1.2 mol% of ICG in MLPs efficiently accelerated drug release and contributed to synergistic therapy of DOX and TAIII without unexpected normal tissue damage.

The orthotopic hepatoma-bearing mice model was thought to be similar to clinical hepatic carcinoma. The photothermal conversion effect of ICG relies on appropriate near-infrared irradiation. However, the penetrating power of infrared light is weak and it is difficult to stimulate deep tissue.[50,51] In the orthotopic transplantation tumor model, near-infrared irradiation is unlikely to penetrate skin and reach HCC cells in liver. Therefore, ICG and MLPs containing ICG were not given to mice and we just evaluated the synergistic therapeutic effect of TAIII and DOX on the orthotopic transplantation tumor model. No serious reduction in body weight was observed in all groups (Figure 8A). To visually monitor tumor growth, the HCC-LM3 cell line stably expressing the firefly luciferase gene was applied taking advantage of its extremely sensitive detection signals and real-time bioluminescence measurement. An IVIS Lumina XR imaging system was used to evaluate tumor growth in orthotopic hepatoma-bearing mice by measuring bioluminescence from HCC-LM3 cells (Figure 8B and C). Tumors were confirmed to be successfully implanted in the livers by detecting bioluminescence after 2 d, as displayed in Figure 8B. TAIII-DOX-LPs significantly inhibited the in vivo growth of HCC-LM3 cells as measured by the

Table 4 Effect of Laser Irradiation on Cell Viability (%) Treated with TAIII-DOX-LPs and MLPs

Concentration	TAIII-DOX-LPs		Concentration	MLPs	
	Laser-	Laser+		Laser-	Laser+
C_1 (DOX=1μM, TAIII=4μM)	67.3±2.6	70.3±5.0	C_1 (DOX=1μM, TAIII=4μM, ICG=1μM)	64.7±2.1	32.9±6.2**
C_2(DOX=2μM, TAIII=8μM)	11.1±2.2	8.6±1.6	C_2(DOX=2μM, TAIII=8μM, ICG=2μM)	10.0±2.6	1.7±2.5**

Notes: **P < 0.01, compared to laser-.

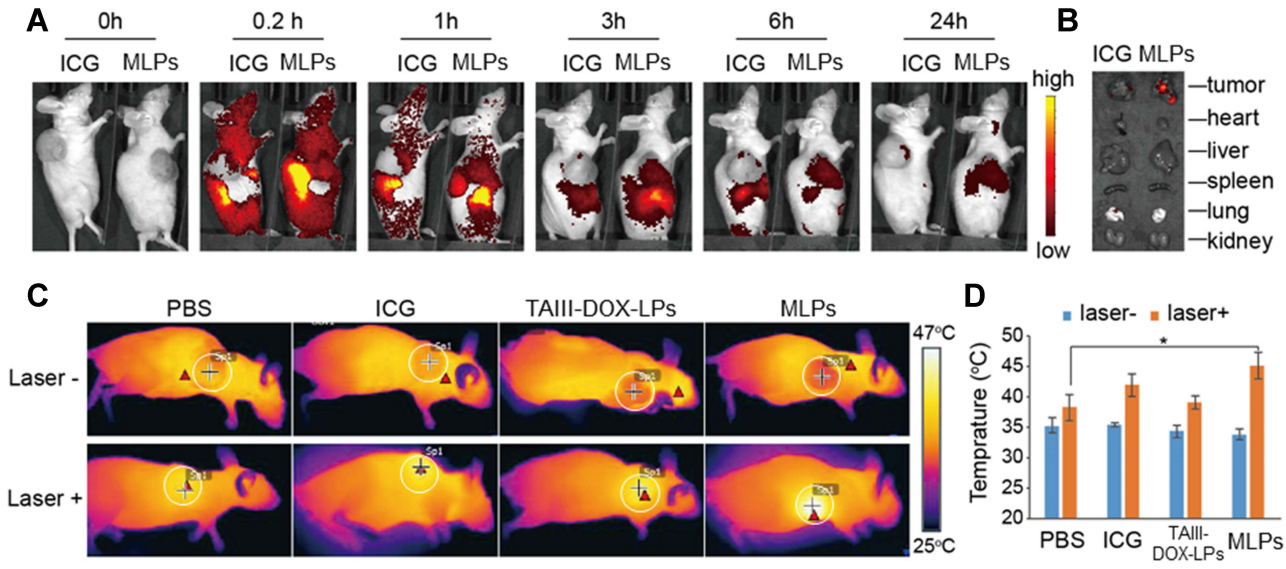

Figure 6 In vivo biodistribution and photothermal imaging. (**A**) In vivo biodistribution imaging of HepG2 tumor–bearing mice after tail vein injection of ICG and MLPs at 0, 0.2, 1, 3, 6, and 24 h. (**B**) Ex vivo fluorescence images of major organs and tumors obtained after 24h-injection. (**C**) Thermal images of HepG2 tumor–bearing mice recorded by an infrared thermal camera before and after tumors were exposed to an 808-nm laser with a 10-min postinjection. (**D**) Temperature of tumor site before and after tumors were exposed to an 808-nm laser with a 10-min postinjection. *$P < 0.05$.

IVIS (Figure 8D) and tumor volume (Figure 8E). The growth inhibitory rates of TAIII-DOX-LPs were 48.2% ± 9.2% as calculated by tumor volume and 56.4% ± 20.7% as calculated by bioluminescence intensity (Table 5). The difference was reasonable because bioluminescence could only be detected in HCC-LM3 cells while the tumor comprised HCC-LM3 cells and interstitium such as the fibrillar connective tissue. Bioluminescence intensity was thought to accurately reflect the actual proliferation of HCC-LM3 cells, and tumor volume was suitable for evaluating tumor growth in vivo. The growth inhibitory rates of TAIII-DOX-LPs calculated by the two methods were higher than that of DOX and TAIII-LPs used alone. The growth inhibitory rate of TAIII-DOX-LPs was 2.6-fold that of DOX (18.3% ± 7.0%) and 3.5-fold that of TAIII-LP (13.8% ± 4.4%) as calculated by tumor volume, and it was 1.9-fold that of DOX (29.3% ± 15.7%) and 1.2-fold that of TAIII-LP (45.4% ± 14.2%) as calculated by bioluminescence intensity. In addition, TAIII-DOX-LPs with 2 mg/kg of DOX exhibited more favorable tumor inhibition than did 5 mg/kg of DOX (27.9% ±21.7%) as calculated by bioluminescence intensity. The results were consistent with the in vivo growth inhibitory activity of MLPs on HepG2 tumor-bearing mice and revealed that DOX and TAIII codelivery liposomes could efficiently improve antitumor activity with synergistic effects on subcutaneous and orthotopic transplantation tumor models.

The TUNEL assay was used to evaluate apoptosis by detecting DNA fragmentation in the nucleus of tumor tissues. As displayed in Figures 7E and 8F, apoptotic tumor cells with brown were observed in HepG2-bearing mice treated with MLPs combined with NIR laser irradiation and HCC-LM3-bearing mice treated with TAIII-DOX-LPs, along with a high inhibitory effect on tumor growth. Treatments with 2 mg/kg, and 5 mg/kg of free DOX and TAIII-LP showed less tumor necrosis signals in subcutaneous and orthotopic transplantation tumor models. Furthermore, H&E staining images of tumors (Figure S5) in the control group were observed with large, irregularly shaped nuclei, with some even being binucleolate, which indicated cell proliferation in tumors. By contrast, tumors treated with MLPs and DOX (5 mg/kg), particularly in the MLPs and NIR laser irradiation group, presented scattered nuclei, clear nuclear shrinkage, and cytoplasmic vacuolation, which indicated tumor tissue necrosis. H&E staining images of the hearts from different treatment groups are displayed in Figures 7F and 8G. As marked by the arrow, obvious histopathologic changes in the cardiac muscle of DOX (5 mg/kg) treated mice (both HepG2 and HCC-LM3 tumor-bearing mice), such as eosinophilic cytoplasm, atrophy cardiac myocytes, inflammatory infiltration, edema, and necrosis were observed. In addition, none of the other treatment groups exhibited significant toxicity in the hearts in contrast to the control group. Other major organs such as the liver, spleen, lung, and kidney in all

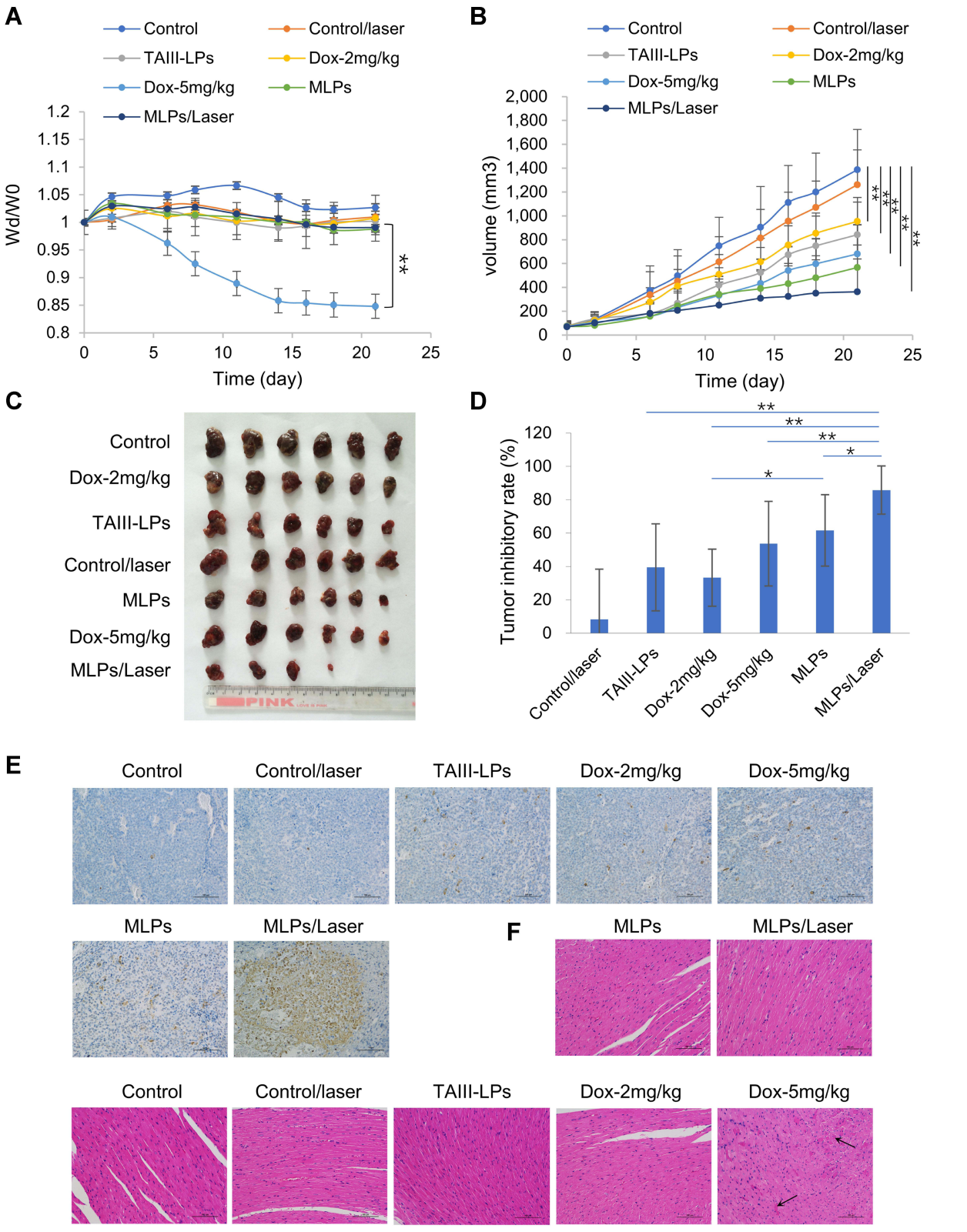

Figure 7 In vivo antitumor evaluation of HepG2-bearing mice after intravenous injection of PBS (shown as the control), free DOX, TAIII-LPs, MLPs, and MLPs with laser irradiation. (**A**) Changes in body weight rate (W_d/W_0). (**B**) Changes in tumor volume rate (V_d/V_0). (**C**) Photograph of tumors excised from mice at Day 21. Day 0 is the day of first injection. (**D**) Tumor-inhibiting rate (%) at Day 21 after the mice were sacrificed. Data are presented as mean ± SD (n = 6).(**E**) TUNEL staining of tumors excised from HepG2 tumor-bearing mice. (**F**) Histological characteristics of hearts excised from HepG2 tumor-bearing mice. Scale bar =100μm. *$P < 0.05$. **$P < 0.01$.

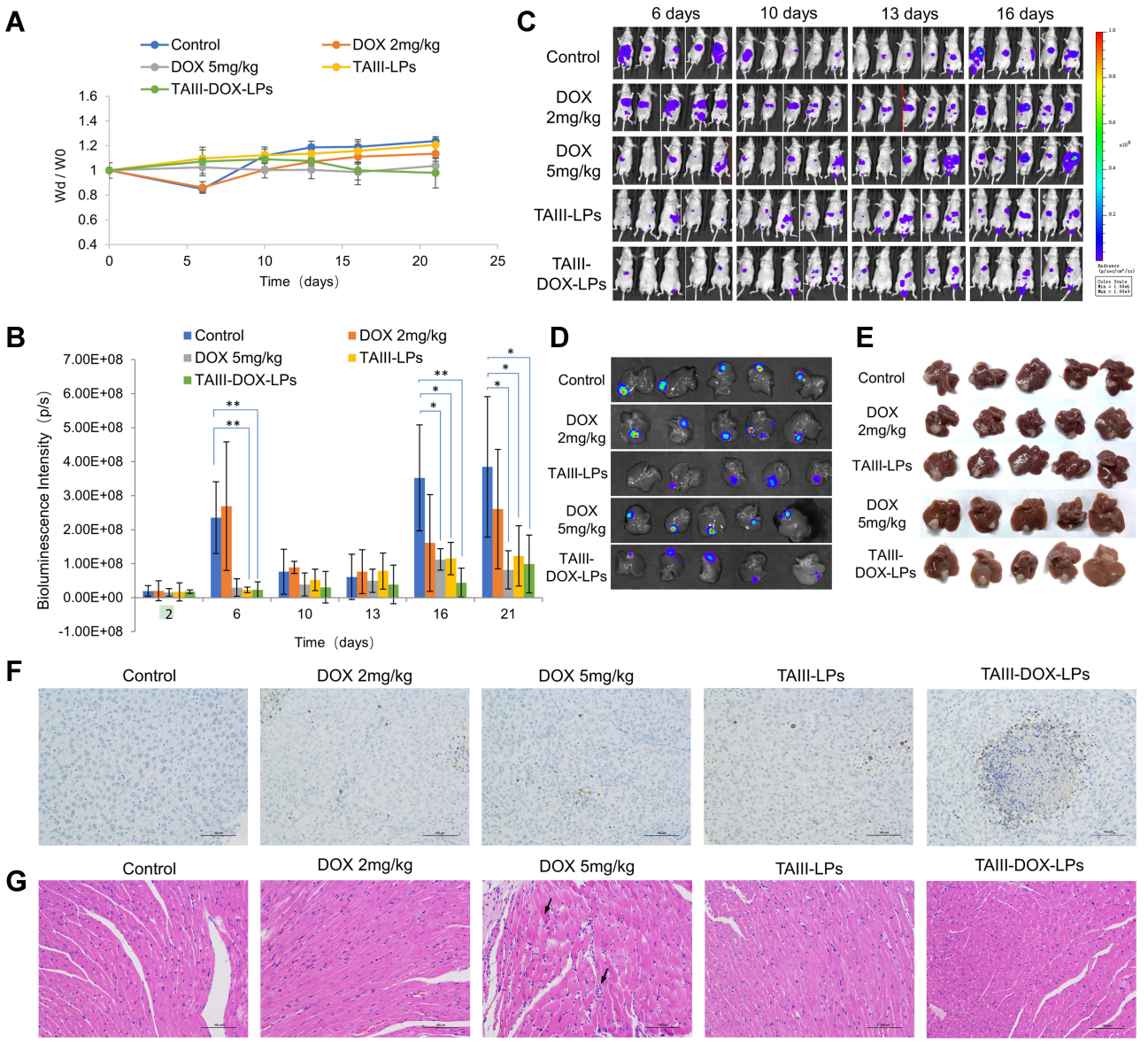

Figure 8 In vivo antitumor evaluation of HCC-LM3-bearing mice after intravenous injection of PBS (shown as the control), free DOX, TAIII-LP, and TAIII-DOX-LPs. (**A**) Changes in body weight rate (W_d/W_0) of each group. (**B**) Bioluminescence intensity of HCC-LM3-bearing mice during the injection period. (**C**) Bioluminescence images of HCC-LM3-bearing mice during the injection period. (**D**) Bioluminescence image of tumors excised from HCC-LM3-bearing mice. (**E**) Photograph of tumors excised from HCC-LM3-bearing mice. (**F**) TUNEL staining of tumors excised from HCC-LM3 tumor-bearing mice. (**G**) Histological characteristics of hearts excised from HCC-LM3 tumor-bearing mice. Scale bar =100μm. *$P < 0.05$. **$P < 0.01$.

groups did not exhibit significant toxicity (Figures S5 and S6). These results revealed that TAIII-based liposomes not only enhanced antitumor effects from the synergies of DOX and TAIII but also reduced side effects from DOX with a lower dosage.

Conclusion

In summary, a novel TAIII-based thermally sensitive liposome formulation to deliver DOX was introduced to achieve synergistic therapeutic effects from TAIII and DOX. Additional ICG loading in MLPs helps induce mild hyperthermia (40–45°C) and initiate burst drug release at tumor sites, which significantly improved the antitumor efficacy of MLPs. TAIII-based multifunctional liposomes not only overcome the limitation of poor solubility and low bioavailability, but also result the significantly enhanced antitumor activity with a low DOX dose and nontoxicity. The innovative application of TAIII

Table 5 The Growth Inhibitory Rates of Each Group on the Orthotopic Transplantation Tumor Model. (n = 6)

Groups	Calculated by Tumor Volume	Calculated by Bioluminescence Intensity
DOX 2 mg/kg	18.3% ± 7.0%	29.3% ± 15.7%
TAIII-LPs	13.8% ± 4.4%	45.4% ± 14.2%
DOX 5 mg/kg	49.7% ± 10.2%	27.9% ±21.7%
TAIII-DOX-LPs	48.2% ± 9.2%*#	56.4% ± 20.7%*

Notes: *P < 0.05, compared to DOX 2mg/kg. #P < 0.05, compared to TAIII-LPs.

working as bilayer stabilizer has never been explored before, which may be referred for the development of other types of saponins with similar structure.

Abbreviations

DOX, doxorubicin hydrochloride; TAIII, timosaponin AIII; ICG, indocyanine green; PTT, photothermal therapy; NIR, near-infrared light; DPPC, 1,2-Dipalmitoyl-sn-glycero-3-phosphatidylcholine; DSPE-PEG2000, 1,2-Distearoyl-sn-glycero-3- phosphoethanolamine-N-methoxypoly-ethylene glycol 2000; CI, combination index; CCK-8, cell counting kit-8 assay; TAIII-DOX-LPs, TAIII based thermally sensitive liposomes carrying DOX; MLPs, TAIII-based multifunctional thermally sensitive liposomes carrying DOX and ICG; DL, drug loading efficiency; EE, entrapment efficiency; CLSM, confocal laser scanning microscope.

Acknowledgments

This work was supported by programs of the National Natural Science Foundation of China [grant number 81872981]; "Shuguang Program" supported by Shanghai Education Development Foundation and Shanghai Municipal Education Commission [grant numbers 20SG43]; The Key project of Shanghai 3-year plan [grant number ZY(2018–2020)-CCCX-2001-04]; The National Scientific and Technological Major Special Project of China [grant number 2019ZX09201004-002]; The projects sponsored by the development fund for Shanghai talents [grant number 2018105]; Youth Talent Sail Plan from the Shanghai Committee of Science and Technology [grant number 19YF1449000]; Program of Shanghai Academic/Technology Research Leader [grant number 18XD1403700]; Shanghai Science and technology innovation project [grant number 20S21902500]; program of Shanghai Leading Talents (grant number 2019100); the Innovation activity plan for College Students of SHUTCM [grant number 2020SHUTCM131].

Disclosure

The authors declare no conflicts of interest for this work.

References

1. Bulbake U, Doppalapudi S, Kommineni N, Khan W. Liposomal formulations in clinical use: an updated review. *Pharmaceutics*. 2017;9(4):12. doi:10.3390/pharmaceutics9020012
2. Ercole F, Whittaker MR, Quinn JF, Davis TP. Cholesterol modified self-assemblies and their application to nanomedicine. *Biomacromolecules*. 2015;16(7):1886–1914.
3. Allen TM, Cullis PR. Liposomal drug delivery systems: from concept to clinical applications. *Adv Drug Deliv Rev*. 2013;65(1):36–48.
4. Efimova AA, Kostenko SN, Orlov VN, Yaroslavov AA. Effect of cholesterol on the phase state and permeability of mixed liposomes composed of anionic diphosphatidylglycerol and zwitterionic dipalmitoylphosphatidylcholine. *Mendeleev Commun*. 2016;26(2):99–100. doi:10.1016/j.mencom.2016.03.003
5. Wang C, Siriwardane DA, Jiang W, Mudalige T. Quantitative analysis of cholesterol oxidation products and desmosterol in parenteral liposomal pharmaceutical formulations. *Int J Pharm*. 2019;569:118576. doi:10.1016/j.ijpharm.2019.118576
6. Carr BI, Giannelli G, Guerra V, et al. Plasma cholesterol and lipoprotein levels in relation to tumor aggressiveness and survival in HCC patients. *Int J Biol Markers*. 2018;33(4):423–431. doi:10.1177/1724600818776838
7. McDonnell DP, Park S, Goulet MT, et al. Obesity, cholesterol metabolism, and breast cancer pathogenesis. *Cancer Res*. 2014;74(18):4976–4982. doi:10.1158/0008-5472.CAN-14-1756
8. Lin CY, Huo C, Kuo LK, et al. Cholestane-3 beta, 5 alpha, 6 beta-triol suppresses proliferation, migration, and invasion of human prostate cancer cells. *PLoS One*. 2013;8(6):18.
9. Wang C, Li P, Xuan J, et al. Cholesterol enhances colorectal cancer progression via ROS elevation and MAPK signaling pathway activation. *Cell Physiol Biochem*. 2017;42(2):729–742. doi:10.1159/000477890
10. Kuzu OF, Noory MA, Robertson GP. The role of cholesterol in cancer. *Cancer Res*. 2016;76(8):2063–2070. doi:10.1158/0008-5472.CAN-15-2613
11. Beckwitt CH, Brufsky A, Oltvai ZN, Wells A. Statin drugs to reduce breast cancer recurrence and mortality. *Breast Cancer Res*. 2018;20(1):144. doi:10.1186/s13058-018-1066-z
12. Sharma A, Bandyopadhayaya S, Chowdhury K, et al. Metformin exhibited anticancer activity by lowering cellular cholesterol content in breast cancer cells. *PLoS One*. 2019;14(1):e0209435. doi:10.1371/journal.pone.0209435
13. Cagel M, Grotz E, Bernabeu E, Moretton MA, Chiappetta DA. Doxorubicin: nanotechnological overviews from bench to bedside. *Drug Discov Today*. 2017;22(2):270–281. doi:10.1016/j.drudis.2016.11.005

14. Zhu Y-J, Zheng B, Wang H-Y, Chen L. New knowledge of the mechanisms of sorafenib resistance in liver cancer. *Acta Pharmacol Sin*. 2017;38(5):614–622. doi:10.1038/aps.2017.5
15. Xu X, Ho W, Zhang X, Bertrand N, Farokhzad O. Cancer nanomedicine: from targeted delivery to combination therapy. *Trends Mol Med*. 2015;21(4):223–232. doi:10.1016/j.molmed.2015.01.001
16. Dutta S, Mahalanobish S, Saha S, Ghosh S, Sil PC. Natural products: an upcoming therapeutic approach to cancer. *Food Chem Toxicol*. 2019;128:240–255. doi:10.1016/j.fct.2019.04.012
17. Hamza AA, Ahmed MM, Elwey HM, Amin A, Ahmad A. Melissa officinalis protects against doxorubicin-induced cardiotoxicity in rats and potentiates its anticancer activity on MCF-7 cells. *PLoS One*. 2016;11(11):e0167049. doi:10.1371/journal.pone.0167049
18. Al-Hrout A, Chaiboonchoe A, Khraiwesh B, et al. Safranal induces DNA double-strand breakage and ER-stress-mediated cell death in hepatocellular carcinoma cells. *Sci Rep*. 2018;8(1):16951. doi:10.1038/s41598-018-34855-0
19. Ashktorab H, Soleimani A, Singh G, et al. Saffron: the golden spice with therapeutic properties on digestive diseases. *Nutrients*. 2019;11 (5):943. doi:10.3390/nu11050943
20. Zhao Y-Z, Zhang -Y-Y, Han H, et al. Advances in the antitumor activities and mechanisms of action of steroidal saponins. *Chin J Nat Med*. 2018;16(10):732–748. doi:10.1016/S1875-5364(18)30113-4
21. Fuchs H, Bachran D, Panjideh H, et al. Saponins as tool for improved targeted tumor therapies. *Curr Drug Targets*. 2009;10(2):140–151. doi:10.2174/138945009787354584
22. Han FY, Song XY, Chen JJ, Yao GD, Song SJ. Timosaponin AIII: a novel potential anti-tumor compound from anemarrhena asphodeloides. *Steroids*. 2018;140:125–130. doi:10.1016/j.steroids.2018.09.014
23. Wang Y, Xu L, Lou LL, et al. Timosaponin AIII induces apoptosis and autophagy in human melanoma A375-S2 cells. *Arch Pharm Res*. 2017;40(1):69–78. doi:10.1007/s12272-016-0763-3
24. Jung O, Lee J, Lee YJ, et al. Timosaponin AIII inhibits migration and invasion of A549 human non-small-cell lung cancer cells via attenuations of MMP-2 and MMP-9 by inhibitions of ERK1/2, Src/FAK and beta-catenin signaling pathways. *Bioorg Med Chem Lett*. 2016;26 (16):3963–3967. doi:10.1016/j.bmcl.2016.07.004
25. Lim SM, Jeong JJ, Kang GD, Kim KA, Choi HS, Kim DH. Timosaponin AIII and its metabolite sarsasapogenin ameliorate colitis in mice by inhibiting NF-kappa B and MAPK activation and restoring Th17/Treg cell balance. *Int Immunopharmacol*. 2015;25 (2):493–503. doi:10.1016/j.intimp.2015.02.016
26. Wang H-Q, Gong X-M, Lan F, et al. Biopharmaceutics and pharmacokinetics of timosaponin A-III by a sensitive HPLC-MS/MS method: low bioavailability resulting from poor permeability and solubility. *Curr Pharm Biotechnol*. 2020.
27. Lin Y, Zhao W-R, Shi W-T, et al. Pharmacological activity, pharmacokinetics, and toxicity of timosaponin AIII, a natural product isolated fromanemarrhena asphodeloidesbunge: a review. *Front Pharmacol*. 2020;11. doi:10.3389/fphar.2020.00764
28. Lorent JH, Quetin-Leclercq J, Mingeot-Leclercq M-P. The amphiphilic nature of saponins and their effects on artificial and biological membranes and potential consequences for red blood and cancer cells. *Org Biomol Chem* 2014;12(44):8803–8822. doi:10.1039/C4OB01652A
29. Hong C, Liang J, Xia J, et al. One stone four birds: a novel liposomal delivery system multi-functionalized with ginsenoside Rh2 for tumor targeting therapy. *Nanomicro Lett*. 2020;12(1):1. doi:10.1007/s40820-020-00472-8
30. Lu L, Ding Y, Zhang Y, et al. Antibody-modified liposomes for tumor-targeting delivery of timosaponin AIII. *Int J Nanomedicine*. 2018;13:1927–1944. doi:10.2147/IJN.S153107
31. Guo Y, Zhang Y, Ma J, et al. Light/magnetic hyperthermia triggered drug released from multi-functional thermo-sensitive magnetoliposomes for precise cancer synergetic theranostics. *J Control Release*. 2018;272:145–158. doi:10.1016/j.jconrel.2017.04.028
32. Liu J, Liang H, Li M, et al. Tumor acidity activating multifunctional nanoplatform for NIR-mediated multiple enhanced photodynamic and photothermal tumor therapy. *Biomaterials*. 2017;157:107–124. doi:10.1016/j.biomaterials.2017.12.003
33. Dou Y, Hynynen K, Allen C. To heat or not to heat: challenges with clinical translation of thermosensitive liposomes. *J Control Release*. 2017;249:63–73. doi:10.1016/j.jconrel.2017.01.025
34. Shemesh CS, Moshkelani D, Zhang H. Thermosensitive liposome formulated indocyanine green for near-infrared triggered photodynamic therapy: in vivo evaluation for triple-negative breast cancer. *Pharm Res*. 2015;32(5):1604–1614. doi:10.1007/s11095-014-1560-7
35. Nguyen HT, Tran TH, Thapa RK, et al. Incorporation of chemotherapeutic agent and photosensitizer in a low temperature-sensitive liposome for effective chemo-hyperthermic anticancer activity. *Expert Opin Drug Deliv*. 2017;14(2):155–164. doi:10.1080/17425247.2017.1266330
36. Yoon HJ, Lee HS, Lim JY, Park JH. Liposomal indocyanine green for enhanced photothermal therapy. *ACS Appl Mater Interfaces*. 2017;9 (7):5683–5691. doi:10.1021/acsami.6b16801
37. Lu L, Liu Y, Ding Y, et al. Preparation of highly purified timosaponin AIII from rhizoma anemarrhenae through an enzymatic method combined with preparative liquid chromatography. *Nat Prod Res*. 2016;30(20):2364–2367. doi:10.1080/14786419.2016.1169416
38. Zhang B, Wang T, Yang S, et al. Development and evaluation of oxaliplatin and irinotecan co-loaded liposomes for enhanced colorectal cancer therapy. *J Control Release*. 2016;238:10–21. doi:10.1016/j.jconrel.2016.07.022
39. Camacho KM, Menegatti S, Vogus DR, et al. DAFODIL: a novel liposome-encapsulated synergistic combination of doxorubicin and 5FU for low dose chemotherapy. *J Control Release*. 2016;229:154–162. doi:10.1016/j.jconrel.2016.03.027
40. Shaikh IM, Tan K-B, Chaudhury A, et al. Liposome co-encapsulation of synergistic combination of irinotecan and doxorubicin for the treatment of intraperitoneally grown ovarian tumor xenograft. *J Control Release*. 2013;172(3):852–861. doi:10.1016/j.jconrel.2013.10.025
41. Zhao YZC, Lu L, Wu W, Zhu X, Fan H, Ding Y. Establishment of an nude mouse orthotopic tumor model of human hepatocellular carcinoma with luciferase expression. *Chin J Comp Med*. 2019;29(9):68–74.
42. Ludwig AD, Labadie KP, Seo YD, et al. Yttrium-90-labeled anti-glypican 3 radioimmunotherapy halts tumor growth in an orthotopic xenograft model of hepatocellular carcinoma. *J Oncol*. 2019;2019:1–7. doi:10.1155/2019/4564707
43. Yang Y-F, Xie X-Y, Yang Y, Zhang H, Mei X-G. A review on the influences of size and surface charge of liposome on its targeted drug delivery in vivo. *Yao Xue Xue Bao*. 2013;48(11):1644–1650.
44. Zhang LW, Monteiro-Riviere NA. Mechanisms of quantum dot nanoparticle cellular uptake. *Toxicol Sci*. 2009;110(1):138–155. doi:10.1093/toxsci/kfp087
45. Francis G, Kerem Z, Makkar HPS, Becker K. The biological action of saponins in animal systems: a review. *Br J Nutr*. 2002;88 (6):587–605. doi:10.1079/BJN2002725
46. Sudji IR, Subburaj Y, Frenkel N, Garcia-Saez AJ, Wink M. Membrane disintegration caused by the steroid saponin digitonin is related to the presence of cholesterol. *Molecules*. 2015;20 (11):20146–20160. doi:10.3390/molecules201119682
47. Huang HL, Chiang WL, Hsiao PC, et al. Timosaponin AIII mediates caspase activation and induces apoptosis through JNK1/2 pathway in human promyelocytic leukemia cells. *Tumor Biol*. 2015;36 (5):3489–3497. doi:10.1007/s13277-014-2985-7

48. Sy LK, Yan SC, Lok CN, Man RY, Che CM. Timosaponin A-III induces autophagy preceding mitochondria-mediated apoptosis in HeLa cancer cells. *Cancer Res*. 2008;68(24):10229–10237. doi:10.1158/0008-5472.CAN-08-1983
49. Kang YJ, Chung HJ, Nam JW, et al. Cytotoxic and antineoplastic activity of timosaponin A-III for human colon cancer cells. *J Nat Prod*. 2011;74(4):701–706. doi:10.1021/np1007735
50. Mou Z, You M, Xue W. Gold nanorod-assisted near-infrared stimulation of bullfrog sciatic nerve. *Lasers Med Sci*. 2018;33(9):1907–1912. doi:10.1007/s10103-018-2554-1
51. Romano A, Ho JS. Microwave to near-infrared conversion with a millimeter-scale wireless laser for activating molecular transducers. *Annu Int Conf IEEE Eng Med Biol Soc*. 2016;2016:352–354. doi:10.1109/EMBC.2016.7590712